DOI: 10.61782/fa.2025.0378

FORUM ACUSTICUM
EURONOISE 2025

EXPERIMENTAL MODAL ANALYSIS OF A CROSS-LAMINATED TIMBER L-JUNCTION WITH A VIEW TOWARDS PREDICTING FLANKING SOUND TRANSMISSION

Sven Vallely[1,2*] **Antonio Esposito**[1] **Stefan Schoenwald**[1]
[1]Laboratory for Acoustics / Noise Control, Empa, Switzerland
[2]Department of Civil Engineering – Structural Mechanics Section, KU Leuven, Belgium

ABSTRACT

The trend towards engineered wood and, as a result, lightweight constructions has led to noise and vibration design challenges. One such challenge that is currently an active research topic is flanking sound transmission through connected building elements. Mass timber buildings are typically formed by connecting cross-laminated timber panels, whereby the type and number of joints used to form a connection can vary depending on the design and purpose of the building. The variety of connector types and implementations poses challenges for the prediction process. Moreover, the connection of the simpler panel subsystems gives rise to emergent behaviour, resulting in a complex dynamic system. As a first step, to better predict flanking sound transmission and to correctly simulate the junction mechanics in vibroacoustic numerical models, it is important to understand the emergent dynamic behaviour due to the connection of these structural elements. This contribution presents a detailed experimental modal analysis of a scaled cross-laminated timber L-junction structure. The mock-up is considered representative of a cross-section that would be encountered in the practice. The experimental modal analysis examines three different L-junction configurations to deduce the contribution of both the brackets and the resulting contacting panel interfaces to the system's dynamic behaviour.

Keywords: *CLT, modal analysis, connection, FEM, acoustics*

**Corresponding author*: *sven.vallely@empa.ch.*

1. INTRODUCTION

Due to its lightweight yet stiff nature, Cross-Laminated Timber (CLT) is a popular structural element choice for the construction of mass timber buildings. While this property is generally beneficial, it poses vibration serviceability and acoustic design challenges.

One approach to help address these challenges is the development of methods and models to characterise and predict the behaviour of CLT structures. This has been considered at several scales, from individual elements [1–3] to operational mid-rise structures [4, 5]. While each modelling scale has its own challenges, modelling at a junction scale has a unique challenge since, here, not just material properties play a crucial role but also the intricate dynamics of the connections [6].

This contribution takes an experimental approach to considering the role of connection dynamics with the view of developing models to accurately predict flanking sound transmission across CLT elements. An experiment was designed with the intent to isolate and determine the contributions of the connectors and contact between plate interfaces on the modal response of a system. To achieve this, three structurally isolated L-junction configurations were investigated: (1) An L-junction connection with two standard steel angle brackets and contact between plate interfaces; (2) The same L-junction connection as (1), but with a 3 mm gap between the plate interfaces; (3) The same L-junction as (1), but with no angle brackets.

2. BACKGROUND AND THEORY

In order to compare and correlate the experimentally fitted modes, a shape-based index, namely the Modal Assurance Criterion (MAC), is chosen. The MAC has diverse appli-

cations not just for mode pairing, but also for for eigenmode error analysis [7]. Such an example is the use of the AutoMAC to check against spatial aliasing. For assessing MAC (and AutoMAC) indices, values of 0.9 or greater are considered to be well-correlated eigenmode pairs and values of 0.1 or less are considered to be uncorrelated eigenmode pairs for the purpose of this contribution. Further discussion of the benefits, limitations, and interpretation of this shape-based index can be found in Refs. [7, 8].

3. MATERIALS AND METHODS

3.1 Experimental set-up

The experimental set-up involved vibration measurements of three CLT L-junction configurations. The L-junction configurations were each formed by connecting two 3-ply CLT plates denominated as CLT060C1 and CLT100A1, respectively. The geometrical properties of the plates are presented in Table 1.

Table 1. Geometrical properties of the experimentally investigated plates. Namely length a, width b, individual layer thickness t_i, and lay-up.

Plate ID	a (m)	b (m)	t_i (mm)	Lay-up (°)
CLT100A1	2.87	1.14	[30/40/30]	[90/0/90]
CLT060C1	1.52		[20/20/20]	

A schematic of the L-junction formed by the two plates and the three different configurations is presented in Fig. 1. The three different configurations of the L-junctions were formed by using different joining methods to connect the two plates along their respective short edges, labeled as DA in Fig. 1. The configurations are designated as follows. 0G2B is the case for using two brackets (2B) and contact, that is, a 0 mm gap (0G) between the plates when forming their connection. 3G2B is the case for using two brackets (2B) and no contact, that is, a 3 mm gap (3G) between the plates when forming their connection. 0G0B is the case for using no brackets (0B) and contact, that is, a 0 mm gap (0G) between the plates when forming their connection.

The brackets used to form the connection for configs. 0G2B and 3G2B were standard steel angle brackets with product number. The brackets had global dimensions of $90 \times 90 \times 65 \times 2.5$ mm and were offset 150 mm from the long edge of the plate and fastened with 8 wood screws per bracket. The screws had a thread length of 40 mm and an

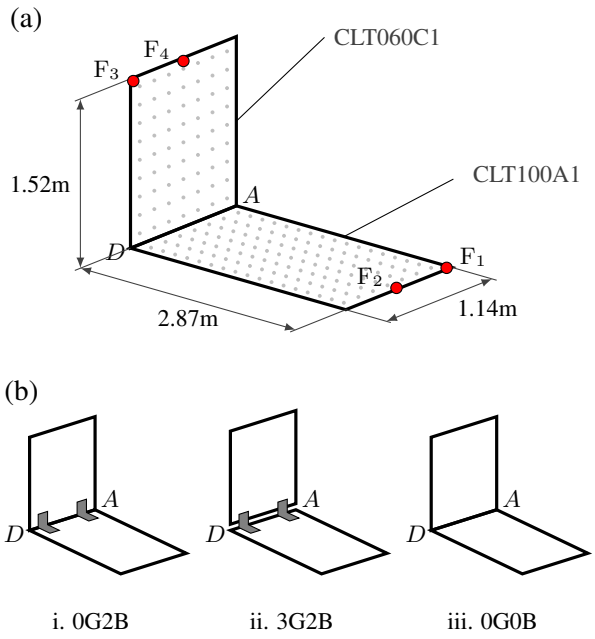

Figure 1. Schematic of the experimental set-up. (a) Schematic of the experimental set-up indicating planar dimensions, approximate measurement grid, and locations of the excitation positions. (b) Schematics of the different joining methods used to connect the two CLT plates along edge DA.

outer thread diameter of approximately 5 mm. An image of an individual bracket is presented in Fig. 3b along with the fixing point locations.

The test structure was supported on four air cushions near the corners of plate CLT100A1 in order to simulate free boundary conditions. The air cushions enabled the test object to be structurally isolated from the ambient environment while minimising the constraint effects of the supports on vibroacoustic behaviour of the system, thereby approximating free boundary conditions.

For the measurement of the vibrational response of the system, a Polytec PSV-400 Laser Doppler Vibrometer measured the normal velocities of the top-side surfaces of plates CLT060C1 and CLT100A1. The measurement grids on plates CLT060C1 and CLT100A1 were 7×9 and 7×17 Cartesian point grids, respectively. These Cartesian point grids corresponded to a spatial resolution of approximately 18 cm. The approximate measurement grids are depicted in Fig. 1a.

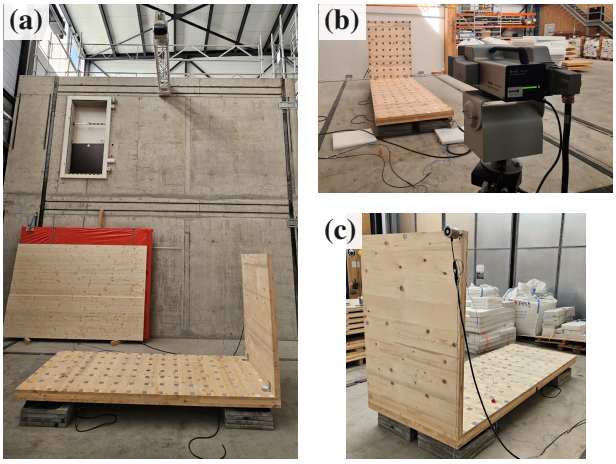

Figure 2. Images of the general experimental set-up: Configuration 0G2B is shown. (a) Acquisition of the normal surface velocities on plate CLT100A1. (b) Acquisition of the normal surface velocities on plate CLT060C1. (c) Rear view with shaker attached.

Four different excitation points were considered, two per plate, with one being approximately on a corner of the plate at the free end, and one being in the middle of the short edge of the plate. The locations of the excitation points are depicted in Fig. 1a. At the excitation points, an impedance head was attached to which a shaker was then attached. The velocity response surface was measured for each excitation point with a swept sine excitation. The transfer mobilites were then calculated based on the measured response surfaces with respect to the force signal of the impedance head. A frequency range from 0 Hz to 800 Hz with a resolution of 62.5 mHz was considered. For each measurement point, the measurements were repeated 5 times for each point, and a complex average was taken.

An overall view of the experimental set-up is presented in Fig. 2, which shows the 0G2B configuration. The 3G2B and 0G0B configurations required slight modification to the structure for safety reasons due to the reduced stability of the connection. For config. 3G2B, plate CLT060C1 was supported from behind with two air cushions. Images of the modification made for config. 3G2B are presented in Fig. 3. For config. 0G0B, guiding cross-bars at the front and back sides were constructed to ensure that plate CLT060C1 did not tip or slide away from its location. CLT060C1 was decoupled from the cross-bars with soft elastic interlayers to ensure that the cross-bars did not influence the vibroacoustic response of the system. The Images of the additional modifications made for config. 0G0B are presented in Fig. 4. It should be stated that the L-junction was constructed so that CLT060C1 was supported as much as possible by CLT100A1 and structurally isolated from the frame which acted as a secondary support.

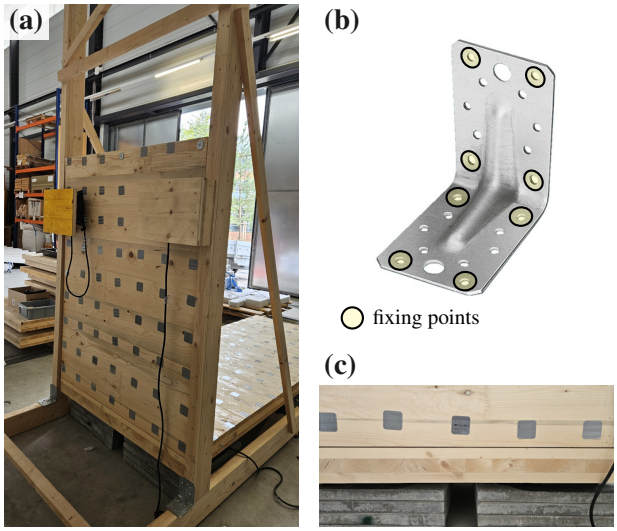

Figure 3. Images of the 3G2B configuration. (a) Rear view of the supporting frame for plate CLT060C1. (b) The angle bracket used to form the connection (also used with config. 0G2B). (c) Close-up view of the 3 mm gap between plate edges.

The measurements for the modal analysis were conducted as part of a broader investigation into flanking sound transmission. See Ref. [9] for details on other excitation points and investigations in the mid- to high-frequency range.

3.2 Modal Parameter Estimation

The experimental modal parameters presented in this contribution were fitted as part of an Experimental Modal Analysis (EMA) using the combined measurement data obtained with the procedure discussed in Sec. 3.1. Further details of the EMA method can found in Ref. [8].

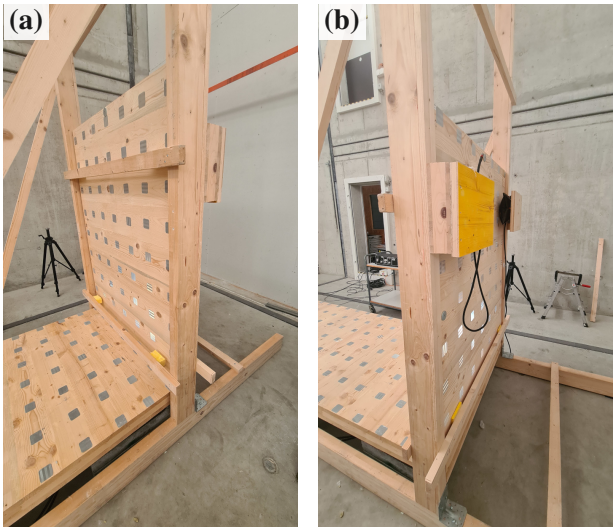

Figure 4. Images of the 0G0B configuration. (a) Front view of the supporting frame for plate CLT060C1. (b) Rear view of the supporting frame for plate CLT060C1.

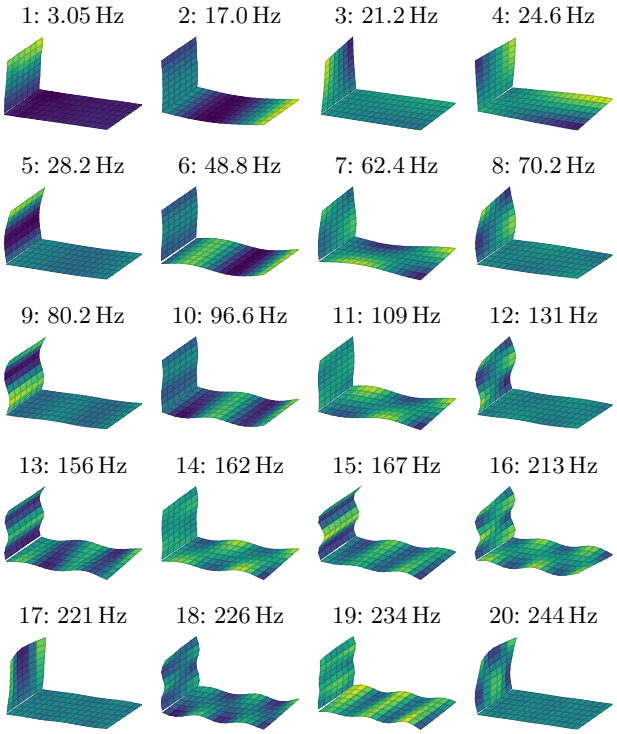

Figure 5. The first twenty identified eigenmodes with their experimental eigenfrequencies for 0G2B.

4. RESULTS AND DISCUSSION

4.1 Modal Parameter Estimation

The EMAs of each of the configurations were able to fit 20 modes for the 0G2B and 3G2B configurations and 18 modes for the 0G0B configuration. The fitted eigenmodes and their associated eigenfrequencies are presented in Figs. 5 to 7. The AutoMAC matrices of the respective eigenmodes are presented in Figs. 8 to 10. The eigenmodes, as expected, correlate exactly with themselves, i.e. $MAC_{i,j} = 1 \quad \forall i = j$ and the off-diagonal terms are mostly zero or uncorrelated, i.e. $MAC_{i,j} < 0.10 \quad \forall i \neq j$. This indicates that the mode parameter estimation is valid and that the eigenmodes contain a sufficient number of degrees of freedom to prevent spatial aliasing. A corollary of this is that the measurement grid is adequate for the identified modes.

There is, however, one pair of modes where the spatial resolution appears to be inadequate. For config. 3G2B, $MAC_{19,20} = 0.65$, indicating a moderate correlation between the modes. Visually comparing eigenmodes 19 and 20 in Fig. 6 confirms this moderate correlation and indicates a potential spatial aliasing. For config. 0G0B, a moderate correlation between modes is also found, with $MAC_{1,6} = 0.50$. Comparing these modes in Fig. 7, there appears to be an adequate spatial resolution to resolve the modes, therefore, the mild correlation is more likely due to coherent noise as a result of non-linearities at the connection caused by the rigid body motion of mode 1. For the remaining non-zero off-diagonal values in Figs. 8 to 10, it is expected that the values would be zero or much closer to zero if the MAC were to be calculated with mass normalised eigenmodes.

4.2 Auto-Comparison and Auto-Correlation of the Experimental Configurations

Considering the identified eigenmodes in Figs. 5 to 7, three different types of modes have been identified by measuring the normal surface velocities of the structure, that is; rigid body modes, torsional modes, and bending modes. The rigid body modes are modes 1 for configs. 0G2B and 3G2B, and modes 1 to 3 for config. 0G0B. The rigid body modes occur at frequencies approximately an order of magnitude lower than the fundamental bending and torsional modes for the 0G2B and 0G0B configura-

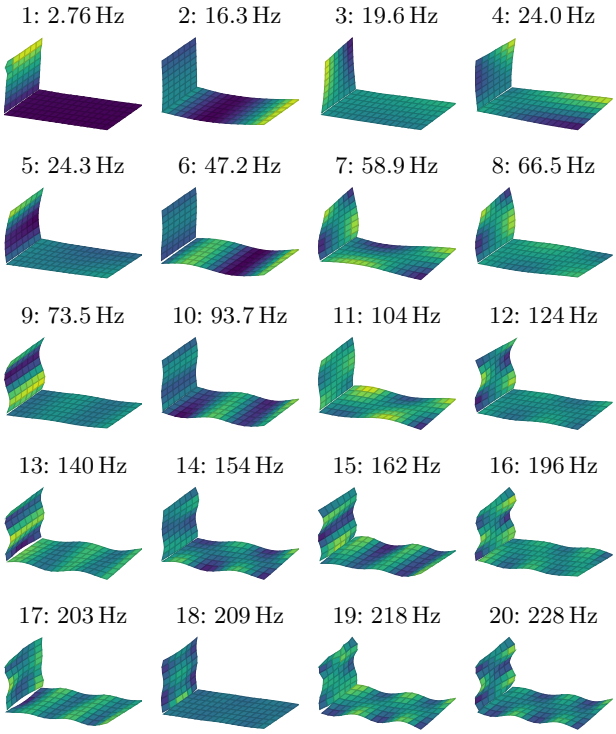

Figure 6. The first twenty identified eigenmodes with their experimental eigenfrequencies for 3G2B.

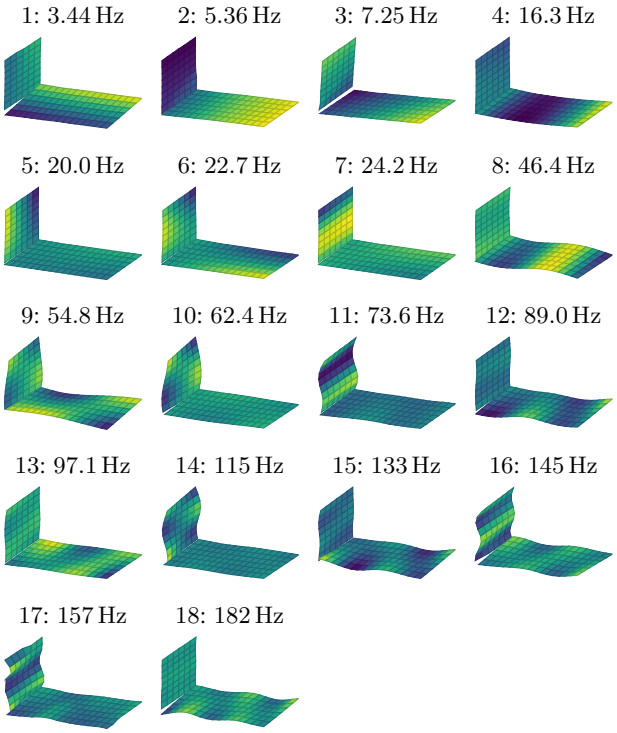

Figure 7. The first twenty identified eigenmodes with their experimental eigenfrequencies for 0G0B.

tions. These rigid body modes are associated with the deformation of the angle bracket and, in conjunction, can potentially provide valuable information for structural identification of the stiffness and damping properties of the connection. The three rigid body modes identified for config. 0G0B have higher eigenfrequencies than those of configs. 0G2B and 3G2B with the steel angle brackets. This result, at a surface level, indicates that the connection is stiffer for 0G0B; however, this additional stiffness is likely due plate CLT060C1 interacting with its supporting structure than with the joining method or, rather, lack there of. A quick visual comparison between the different configurations indicates that the torsional and bending modes do not appear to be influenced by, or at most, negligibly influenced by the supporting structure.

Considering the torsional and bending modes across Figs. 5 to 7, there appears to be cases where the individual plate modes are uncoupled, and other cases where the individual plate modes couple. An example of uncoupled individual plate modes are modes 2 and 5 in Fig. 5. On the other hand, an example of coupled individual plate modes are 13 and 15. What is particularly interesting about these coupled modes, is that they are composed of the same two individual plate modes when considering the plates as individual structural subsystems; however, considering their AutoMAC values, $AutoMAC_{13,15} = 0.05$ (cf. Fig 8), the two modes can be considered uncorrelated. The connection of these two subsystem gives rise to emergent behaviour, whereby they are coupled and moving in phase with respect to each other for mode 13, and coupled and moving out of phase with respect to each other for mode 15, resulting in an approximately 7 % shift in the eigenfrequency. This result of identifying coupling and non-coupling modes could potentially open new possibilities for addressing low-frequency flanking sound transmission. While not a standalone noise control solution, the identification of coupling modes during the design phase of a building could potentially allow for an approach to address problem frequencies for flanking sound transmission without adding additional mass to the structure. For example, by changing of aspect ratios of elements to minimise coupling across the connection, or changing the connec-

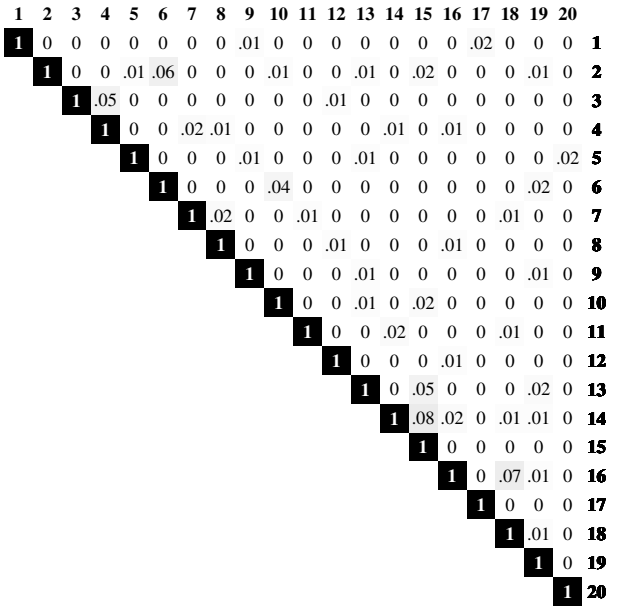

Figure 8. AutoMAC matrix for 0G2B. The colourmap is a linear scale from white ($MAC = 0$) to black ($MAC = 1$).

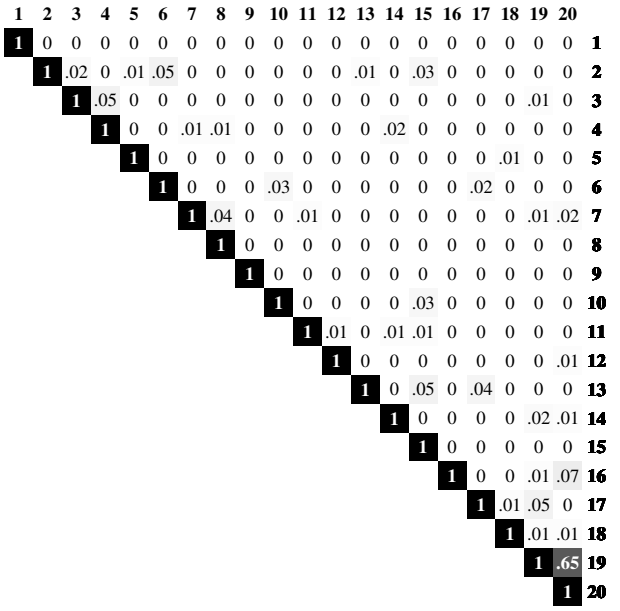

Figure 9. AutoMAC matrix for 3G2B. The colourmap is a linear scale from white ($MAC = 0$) to black ($MAC = 1$).

tion itself.

4.3 Cross-Comparison and Cross-Correlation of the Experimental Configurations

The MAC matrix is computed for each of the three considered experimental configurations against each other in Figs. 11 to 13.

For Fig. 11, where config. 3G2B is compared against config. 0G2B, it can be seen that the eigenmodes of both of the configurations occur in the same order and are well correlated up to the 12$^{\text{th}}$ mode, that is $MAC_{i,j} > 0.9 \quad \forall i = j \in \{1, ..., 12\} : i, j \in \mathbb{N}$. Considering the eigenfrequencies of these well-correlated mode pairs in Figs. 5 and 6, it can be seen that the eigenfrequencies for config. 0G2B are approximately 5 % higher than those of config. 3G2B. This result implies an overall global increase in stiffness of the structure to the effect of approximately 25 % due to the contact at the plate interfaces. This stiffening is even seen when when a resonance of one plate occurs uncoupled from the other, for example with modes 2 and 4. After the 12$^{\text{th}}$ mode, the eigenmode pairs are less well correlated. These results indicate that the brackets most important for coupling of the junction at lower frequencies, but the contact starts to have a greater influence on the response of the system as the frequency range increases.

For Fig. 12, where config. 0G0B is compared against config. 0G2B, it can be seen that the eigenmodes the configurations differ more than with the 3G2B-0G2B case. The modes do not occur in the same order, but this is largely due to the identification of the additional rigid body modes in the 0G0B case. Otherwise, it can be said that the significantly correlated eigenmode pairs occur in the same order. Their are 5 well-correlated mode pairs, that is, the mode pairs with indices $i, j \in \{\{4, 2\}, \{5, 3\}, \{8, 6\}, \{9, 7\}\}$. A general observation that can be made, is that the correlation between mode pairs is generally good for uncoupled plate modes.

Considering Fig. 11 where config. 0G0B is compared against config. 3G2B, it can be seen that the correlation between systems improves, with 8 well-correlated eigenmode pairs. The well-correlated pairs have indices $i, j \in \{\{4, 2\}, \{5, 3\}, \{6, 4\}, \{7, 5\}, \{8, 6\}, \{9, 7\}, \{10, 8\}, \{11, 9\}\}$. As with the case for Fig. 12, the correlation between mode pairs is good for uncoupled plate modes, but the correlation drops off once coupled plate modes start occurring. This implies that for the first several modes

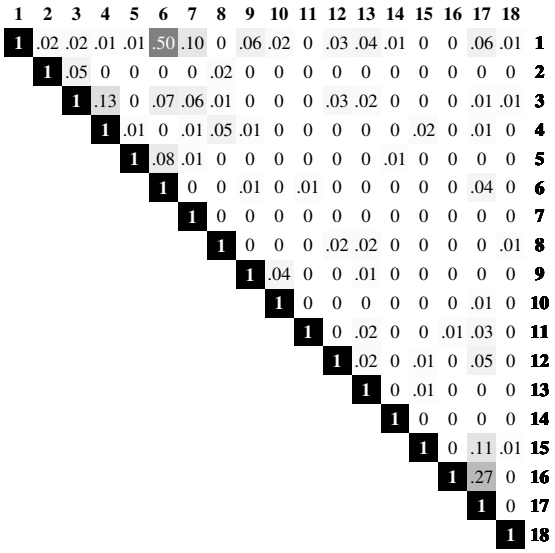

Figure 10. AutoMAC matrix for 0G0B. The colourmap is a linear scale from white ($MAC = 0$) to black ($MAC = 1$).

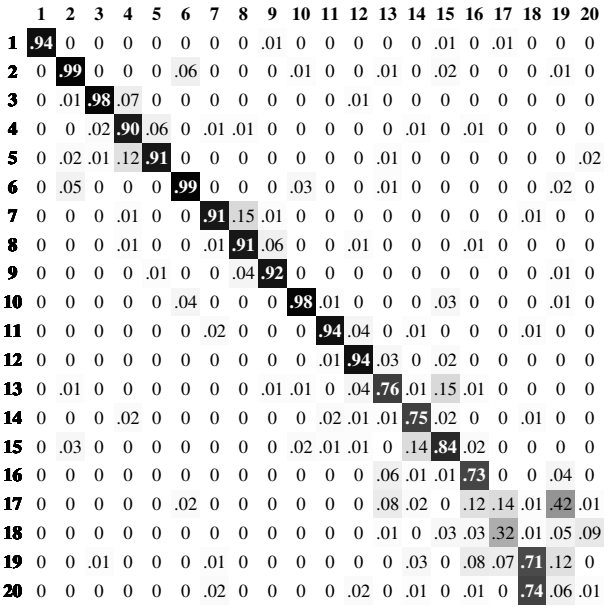

Figure 11. MAC matrix of 3G2B (vertical axis) against 0G2B (horizontal axis) eigenmodes. The colourmap is a linear scale from white ($MAC = 0$) to black ($MAC = 1$).

where the plate subsystems are generally resonating independent of each other, the type of connection doesn't appear to play a large role in influencing the eigenmodes, but does play a moderate role in influencing the global stiffness of the system. However, once the modes of the plate subsystems start coupling, the connection type starts to change the behaviour of the system.

5. SUMMARY AND CONCLUSION

This contribution compares and correlates experimentally estimated modal parameters for three CLT L-junction configurations with the goal of better understanding the behaviour at element interfaces for predicting flanking sound transmission. Each configuration used the same two CLT plates, but the plates in each configuration were connected with slightly different joining methods. The first method involved using two commercially available steel angle brackets supporting one plate resting on top of the other. The second configuration was the top plate supported solely by the angle brackets, thus eliminating any contact between the plates. The third configuration was just the top plate resting on the top plate without angle brackets. These three experimental configurations allowed for the components that form the connection between a typical L-junction, for example, the surface contact between two connected elements and their joining mechanism, to be analysed in a deductive manner.

The analysis identified three different types of modes, namely rigid body, torsional, and bending modes that contribute to the normal response of the L-junction structure. It was found that rigid body modes with the angle brackets could be potentially used for structural identification purposes of the connection. For the first several bending and torsional modes, where the modal density was relatively low, the resonances of the plate subsystems did not couple with each other. In this region, the type of connection did not have a large influence on the eigenmodes. This implies that for the first several bending and torsional modes, aside from moderate changes in the stiffness of the system, the type of connection does not grossly influence the system's structural response. However, for higher frequencies, the modes of the subsystems start to couple, and the simpler plate subsystems give rise to emergent behaviour. That is, a system formed from the connection of simpler subsystems behaves in a way that is more complex than the individual subsystems would behave on their own. This emergent behaviour is, at first, mostly due to the brackets,

	1	2	3	4	5	6	7	8	9	10	11	12	13	14	15	16	17	18	19	20
1	0	.01	0	**.48**	0	0	.04	0	0	.01	.04	.01	0	0	0	.01	0	.03	0	0
2	.01	0	0	0	0	.02	0	0	0	.01	0	0	0	0	.01	0	0	0	0	0
3	.16	.12	0	.08	.01	.01	0	0	0	.04	.01	.01	.01	0	.01	0	0	0	.04	0
4	0	**.98**	.01	0	0	.05	0	0	0	.01	0	0	.01	0	.02	0	0	0	.01	0
5	0	0	**.96**	.05	0	0	0	0	0	0	0	.01	0	0	0	0	0	0	0	0
6	0	.01	.05	**.84**	.11	0	.01	0	0	0	0	0	0	.01	0	0	0	0	0	0
7	.01	.03	0	.19	**.80**	.01	0	0	0	0	0	0	0	0	0	0	0	0	0	.02
8	0	.05	0	0	.01	**.96**	.02	0	0	.02	0	0	.01	0	0	0	0	0	.02	0
9	0	0	.01	.03	0	.01	**.91**	.04	.01	0	0	0	0	.02	0	0	0	0	0	0
10	0	0	.01	.01	0	0	.01	**.88**	.10	0	0	0	0	0	0	.02	0	.01	0	0
11	0	0	0	.01	0	0	.03	.05	**.88**	0	.01	0	0	0	0	0	0	0	0	0
12	0	0	0	0	0	.04	.05	0	0	**.69**	.21	0	0	.01	.01	.01	0	.02	0	0
13	0	0	0	0	0	.02	.06	0	0	.15	**.72**	0	0	0	.01	.01	0	.01	.01	0
14	0	0	0	0	0	0	0	.02	0	0	0	**.85**	.02	.01	.02	0	0	0	0	0
15	0	.02	0	.01	0	0	0	0	0	.06	.17	0	.33	.20	.01	.01	0	0	0	0
16	0	0	0	0	0	0	0	0	.01	0	.01	.10	.34	.23	.14	.02	0	.02	0	0
17	0	.01	0	.04	0	0	.01	0	.03	.02	0	.05	.21	.02	.34	.16	0	0	.01	0
18	0	0	0	0	0	.01	.01	0	0	0	0	0	.19	.17	0	.25	.01	.22	.01	0

Figure 12. MAC matrix of 0G0B (vertical axis) against 0G2B (horizontal axis) eigenmodes. The colourmap is a linear scale from white ($MAC = 0$) to black ($MAC = 1$).

	1	2	3	4	5	6	7	8	9	10	11	12	13	14	15	16	17	18	19	20
1	0	.01	0	**.47**	.04	0	.03	.01	0	.01	.04	.01	0	0	0	0	0	0	.04	0
2	.03	0	0	0	0	.02	0	0	0	.01	0	0	0	0	.01	0	0	0	0	0
3	.11	.13	0	.06	.03	0	0	0	0	.04	.01	0	0	0	0	.01	.05	0	.02	0
4	0	**.99**	.03	0	0	.05	0	0	0	0	0	0	.01	0	.03	0	0	0	0	0
5	0	0	**.97**	.04	0	0	.01	0	0	0	0	0	0	0	0	0	0	0	0	0
6	0	.01	.08	**.97**	0	0	.01	0	0	0	0	0	0	.01	0	0	0	0	0	0
7	0	.02	0	.02	**.96**	0	0	.01	0	0	0	0	0	0	0	0	0	.01	0	0
8	0	.05	0	.01	0	**.98**	.01	0	0	.02	.01	0	0	0	0	0	.02	0	0	0
9	0	.01	0	.02	0	0	**.92**	0	0	0	0	.01	0	.01	0	0	0	0	0	.01
10	0	0	.01	.02	0	0	.14	**.91**	0	0	0	.01	0	.01	0	0	0	0	0	0
11	0	0	0	.01	0	0	.01	0	**.96**	.01	.01	0	.01	0	0	0	0	0	0	0
12	0	0	0	0	0	.04	.02	.01	0	**.76**	.17	0	0	0	.01	.01	0	0	.02	.01
13	0	0	0	0	0	.02	.03	.01	0	.10	**.79**	0	0	0	.01	.01	.01	0	.02	0
14	0	0	0	0	0	0	0	.02	0	.01	.05	**.84**	0	.02	0	.01	0	0	.01	.02
15	0	.02	0	.01	0	0	0	0	0	.04	.11	.01	.28	**.39**	0	0	0	0	.02	0
16	0	0	0	0	0	0	0	0	.01	0	0	.06	**.60**	.24	.04	0	.03	.02	.01	0
17	0	.01	0	.04	0	0	.01	.01	.03	.03	0	.01	.35	0	.28	.05	.08	.10	0	0
18	0	0	0	0	0	.01	.01	0	0	0	0	0	.02	.20	.01	.29	.04	0	.16	.06

Figure 13. MAC matrix of 0G0B (vertical axis) against 3G2B (horizontal axis) eigenmodes. The colourmap is a linear scale from white ($MAC = 0$) to black ($MAC = 1$).

but as the frequency range increases, the contact between the elements starts to have an increasingly larger influence on the response of the system.

Further, this contribution highlights the potential for new measures in addressing flanking sound transmission performance in the low-frequency range. While the effect of the emergent system behaviour due to the coupling of modes from simpler panel subsystems and their direct influence on flanking sound transmission requires further investigation, these modes, once identified, can be shifted or even partially avoided. This could be accomplished without adding additional mass to the structure, such as by carefully selecting element aspect ratios in the design phase or changing the types of connectors themselves. This could even potentially be done remedially with other available measures, such as changing the stiffness of plates, but potentially at the expense of negatively influencing the radiation efficiency of the structure at higher frequencies.

The results of this contribution could be used as a basis for updating or validating a numerical model, such as in Ref. [9].

6. ACKNOWLEDGMENTS

The presented results were developed within the framework of the cooperative project “Schallschutz im Holzbau” between Lignum and Empa.

7. FUNDING

The authors gratefully acknowledge the financial support of the cooperative research project by the Swiss Federal Office for Environment (FOEN) as part of the “Aktionsplan Holz”.

8. REFERENCES

[1] C. E. Churchill, B. Nusser, and C. Lux, “Calculating the equivalent elastic moduli and their influence on modelling the sound insulation of softwood cross laminated timber (clt),” *Applied Acoustics*, vol. 205, 2023.

[2] S. Vallely and S. Schoenwald, “An efficient analytical method to obtain the homogenised frequency-independent elastic material properties of cross-laminated timber elements,” *Journal of Sound and Vibration*, vol. 546, p. 117424, 2023.

[3] J. Lietzén, V. Kovalainen, M. Kylliäinen, and S. Pajunen, "Computational prediction of impact sound insulation of a full-scale timber floor applying a fem simulation procedure," *Engineering Structures*, vol. 310, p. 118130, 2024.

[4] A. Aloisio, D. Pasca, R. Tomasi, and M. Fragiacomo, "Dynamic identification and model updating of an eight-storey clt building," *Engineering Structures*, vol. 213, p. 110593, 2020.

[5] B. Kurent, B. Brank, and W. K. Ao, "Model updating of seven-storey cross-laminated timber building designed on frequency-response-functions-based modal testing," *Structure and infrastructure Engineering*, vol. 19, no. 2, pp. 178–196, 2023.

[6] S. Moons, R. Lanoye, and E. P. Reynders, "Prediction of flanking sound transmission through cross-laminated timber junctions with resilient interlayers," *Applied Acoustics*, vol. 228, p. 110317, 2025.

[7] R. J. Allemang, "The modal assurance criterion–twenty years of use and abuse," *Sound and vibration*, vol. 37, no. 8, pp. 14–23, 2003.

[8] S. Vallely and S. Schoenwald, "Higher-order modal parameter estimation and verification of cross-laminated timber plates for structural-acoustic analyses," *Acta Acustica*, vol. 8, p. 52, 2024.

[9] A. Esposito, S. Vallely, and S. Schoenwald, "Modelling cross-laminated timber plate connections: A numerical investigation on flanking sound transmission through angle brackets," in *Proceedings of Forum Acusticum*, 2025.